



HAL
open science

Using saponified olive oil to make cost effective calcium carbonate particles superhydrophobic

Louiza Abidi, Frédéric Amiard, N. Delorme, Salim Ouhenia, Alain Gibaud

► To cite this version:

Louiza Abidi, Frédéric Amiard, N. Delorme, Salim Ouhenia, Alain Gibaud. Using saponified olive oil to make cost effective calcium carbonate particles superhydrophobic. *Advanced Powder Technology*, 2022, 33 (2), pp.103399. 10.1016/j.appt.2021.103399 . hal-03554320

HAL Id: hal-03554320

<https://univ-lemans.hal.science/hal-03554320>

Submitted on 22 Jul 2024

HAL is a multi-disciplinary open access archive for the deposit and dissemination of scientific research documents, whether they are published or not. The documents may come from teaching and research institutions in France or abroad, or from public or private research centers.

L'archive ouverte pluridisciplinaire **HAL**, est destinée au dépôt et à la diffusion de documents scientifiques de niveau recherche, publiés ou non, émanant des établissements d'enseignement et de recherche français ou étrangers, des laboratoires publics ou privés.



Distributed under a Creative Commons Attribution - NonCommercial 4.0 International License

Using Saponified Olive Oil to make Cost Effective Calcium Carbonate

Particles Superhydrophobic

Louiza Abidi^{a,b}, Frédéric Amiard^a, Nicolas Delorme^a, Salim Ouhenia^b and Alain Gibaud^{a*}

^aInstitut des Molécules et des Matériaux du Mans, UMR 6283 CNRS, Université du Mans, 72085 Le Mans, cedex 09, France

^bLaboratoire de physico-chimie des matériaux et catalyse, Université de Bejaia, Bejaia 06000, Algérie

* corresponding author : gibaud@univ-lemans.fr

Keyword:

Calcium Carbonate, Olive Oil, Vaterite, Calcite, Aragonite, Superhydrophobic particles

Abstract:

The main goal of this paper is to show that superhydrophobic particles of calcium carbonate can be synthesized at low cost from harmless biocompatible natural products like baking soda (NaHCO_3) and olive oil. Calcium carbonate particles were prepared by precipitating solutions containing CO_3^{2-} and Ca^{2+} ions at two different temperatures 30 °C and 80 °C. These particles were transformed into hydrophobic ones using soap made from olive oil from the region of Kabylie (Algeria). The olive oil was first saponified. Adjusted amounts of this soap were added to the sodium carbonate solution before the precipitation reaction. Several techniques were used to analyze the products of the reaction. Typical polymorphs of CaCO_3 (calcite, aragonite and vaterite) were identified by quantitative analysis of X-ray powder diffraction patterns, giving their crystallite size and atomic fractions. Scanning electron microscopy was used to probe the morphology of the CaCO_3 particles. FT-IR measurements indicated the presence of aliphatic chains in the hydrophobic particles, thereby proving that the calcium carbonate particles were functionalized by soap. The particles which formed were found to be superhydrophobic with a contact angle of up to 175°. Evidence of the efficiency of these particles in oil spill recovery is given.

Introduction:

CaCO_3 exists in several anhydrous crystalline polymorph states among which calcite, aragonite and vaterite differ by their crystal structures [1-3] and occur in order of decreasing thermodynamic stability respectively [4, 5]. These polymorphs play a major role in industrial applications. Calcite is employed as a filler in the paper and rubber industries. In the food industry, CaCO_3 labelled E170 is used as a supplement of Ca^{2+} [6, 7]. Calcite is also considered to be a specific substance that can capture CO_2 and is therefore an interesting material for limiting the green house effect. According to Franco et al, the adsorption of CO_2 and methane as well as their diffusion on the calcite surface are well predicted via molecular dynamics simulation. The effective adsorption action of CO_2 molecules on the calcite surface has been clearly observed at low temperature (Tao et al) [8-10]. After calcite, aragonite is the second most common natural form of CaCO_3 . It is found in nacre where the organization of crystalline platelets leads to extraordinary mechanical properties [11-14]. On the opposite, vaterite, which is metastable in water is rarely found in nature [13, 15-17]. Exceptions are observed in urinary and gallstones and in sea urchins [15, 18]. Vaterite being much more porous than calcite and aragonite makes it the most favorable phase to be used as a host matrix for drug delivery in the pharmaceutical industry but its instability in water is a major drawback [15, 19-21]. The biocompatibility, high specific surface, non-toxicity, porous structure and low density of vaterite have fostered intensive studies for improving its stability in water [22, 23]. In the laboratory, CaCO_3 is usually synthesized by a simple technique called co-precipitation in which two aqueous solutions, one of calcium chloride CaCl_2 (or calcium nitrate $\text{Ca}(\text{NO}_3)_2$) and of sodium carbonate (Na_2CO_3) are mixed [24-27]. Modifications in the synthesis protocol such as temperature variation and additive use (organic or inorganic) affect both the morphology, size and polymorphism of CaCO_3 [1, 14, 28]. The crystallization of calcite, vaterite and aragonite is strongly dependent on the reaction temperature. Calcite and vaterite are regularly obtained at low temperatures. For example, Chen et al. found that pure vaterite could be formed at room temperature by the initial adjustment of the pH of the aqueous CaCl_2 solution. Furthermore, Ogino et al. observed that the CaCl_2 - Na_2CO_3 - NaCl - H_2O reaction system at 30°C and 40°C yielded 75% of vaterite. Chen and Xiang showed that aragonite is formed at high temperatures $T \geq 50^\circ\text{C}$ in the CaCl_2 - NH_4HCO_3 - H_2O reaction system, but the generation of pure aragonite takes place at 80°C [29-32]. CaCO_3 is a good example of a material exhibiting a large variety of different morphologies such as flower-like, fried-egg shape, sphere, needle, spheroidal, hexagonal and rhombohedral, ect... [33-35]. Among these shapes, vaterite

can precipitate as a spheroidal porous particle made of small aggregated nanograins having a typical size of about 35 nm [22]. CaCO_3 particles being hydrophilic impede the adsorption of hydrophobic macromolecules and limit its usefulness in applications such as delivery of hydrophobic drugs [27, 36-40]. Recently, hydrophobic calcium carbonate was prepared with evidence that this material could be used as a selective absorbent of oil spills threatening the environment [38]. In that case, pure stearic and oleic acids were used as hydrophobic molecules to transform the hydrophilic CaCO_3 surface into an hydrophobic one [25, 36, 38]. The use of such functionalizing molecules works very well, but their very high price is a lock for their use on an industrial scale. Worldwide, huge cases of accidental oil spills lead to polluting ocean regions with harmful environmental and economic consequences. The expulsion of BP's Deepwater Horizon Oilrig occurring in 2010 in the Gulf of Mexico caused a release of millions of gallons of oil. To cope with similar damages, ecological and cost-effective techniques must be developed to selectively clean up contaminated water. Many traditional methods have been used, including mechanical separation (using a boom), chemical dispersants, micro-organisms and absorbent materials. Yet, the most popular and simplest treatment is that of absorbent materials. Ideally, the material should be able to adsorb oil, be highly selective, recyclable and non-toxic [38].

In this work, we have focused our attention to making hydrophobic calcium carbonate particles at very low cost using natural ingredients such as baking soda (calcium bicarbonate) and olive oil as initial precursors. The calcium carbonate particles were synthesized by the classic co-precipitation method of mixing a solution of calcium chloride with a solution of sodium carbonate. To produce hydrophobic particles, we used soap made from extra virgin olive oil from in Kabylie (Algeria). Olive oil essentially contains esters of fatty acids like oleic, linoleic and palmitic acids with oleic acid being the major constituent with a content varying between 55 and 83 % [41]. Extra virgin oil used in this work was studied by chromatography and FTIR, and it was found to contain 71.5 % of oleic acid (C18:1), 10.6 % of linoleic acid (C18:2) and 10.4 % of palmitic acid (C16:0) derivatives. In this latter study, the discriminant analysis was used to thoroughly analyze the I.R. spectra [42].

The effect of different masses of soap made from olive oil on the morphology, polymorphism and physical properties of CaCO_3 particles was examined by XRD, FT-IR, and SEM and contact angle measurements. We evidenced that the low-cost production of superhydrophobic particles of CaCO_3 either as vaterite or aragonite is possible from eco-friendly materials. No attempt was made to produce superhydrophobic calcite in this work because 1) the time of residence of particles in the aqueous solution was voluntarily kept short to avoid the

dissolution-recrystallisation process in calcite and 2) the temperatures of precipitation were selected to yield either pure vaterite and pure aragonite. The superhydrophobic character of our particles was tested to recover oil spilling at the surface of water. To the best of our knowledge it is the first time that vaterite and aragonite particles were synthesized using soap from olive oil. This approach could be clearly used in the future to obtain superhydrophobic particles of materials prepared by precipitation in solution.

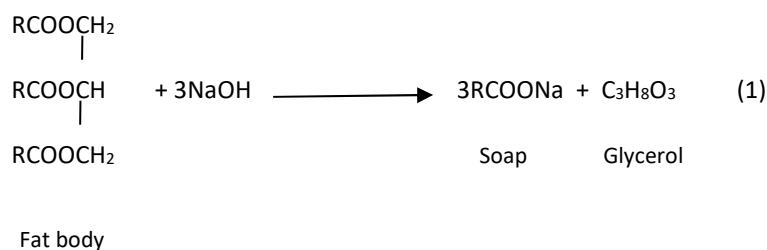
Experimental section:

$\text{CaCl}_2 \cdot 2\text{H}_2\text{O}$ ($\leq 99\%$ pure) from Acros-Organics and commercial NaHCO_3 (99% pure) were used as reagents. NaOH was purchased from Sigma-Aldrich and extra virgin olive oil was taken from the Kabylie region of Bejaia (Algeria).

In a first step, an aqueous solution of Na_2CO_3 was prepared by mixing the reagents NaHCO_3 and NaOH at a concentration of 0.5 M (solution A) in deionized water. This procedure allows to control the pH of the solution and is less expensive than buying Na_2CO_3 . A solution of $\text{CaCl}_2 \cdot 2\text{H}_2\text{O}$, 0.5 M (pH=7.48, 100 ml) was then prepared and kept sealed to avoid any contact with CO_2 from atmosphere (Solution B). Second, a solid soap was made from olive oil. The fatty acid esters contained in olive oil were transformed into carboxylate by saponification with caustic soda. Typically, 10 g of olive oil was added to 1.3 g of NaOH in 3.8 g of water with stirring for 20 - 30 minutes until the mixture became pasty.

This mixture was kept as so for a few days until the soap became hard. A series of soap masses, i.e 0.05 g, 0.1 g, 0.2 g and 0.4 g were weighed and further dissolved in 10 ml of ethanol at a temperature close to 80 °C to facilitate the dissolution of the soap (solution C). After cooling, solution C was poured into 90 ml of Na_2CO_3 (pH = 10.85 solution A) to yield solution D of total volume 100 ml. Solutions B and D were then rapidly mixed at elevated speed (10000 rpm) in a blender at 30 ± 1 °C and 80 ± 1 °C. These two temperatures were chosen because they are known to yield either vaterite and aragonite respectively [18 and references therein]. Note that we have used here a cost-effective commercial blender with a stirring speed of 10000 rpm as the stirrer. Such commercial blenders are readily available and provide high speed stirring capabilities at a controllable temperature which are not achieved with a magnetic stirrer. Since the masses of soap (0g, 0.05g, 0.1g, 0.2g and 0.4g) were dissolved in a total volume of 200 ml, the final concentrations of soap in the mixed solutions B and D were (0 g/L, 0.25 g/L, 0.5 g/L, 1 g/L and 2 g/L).

The effect of caustic soda on the fatty esters of olive oil leading to soap in the form of sodium carboxylates and glycerol is provided in reaction (1).



In the process, the carboxylate are then mixed with the Na_2CO_3 prior to mixing with the CaCl_2 solution. The sodium oleate, sodium linoleate and sodium palmitate obtained by reactions of oleic acid, linoleic acid and palmitic esters with NaOH can bind to Ca^{2+} ions to form Ca-carboxylate as shown in the chemical reaction (2) [38].



Reaction (3) is the chemical reaction of precipitation of calcium carbonate.



Yet, some of the Ca^{2+} ions are bound to carboxylate chains and during the precipitation some of those chains are adsorbed at the surface of the CaCO_3 nanograins and may even be trapped inside the particles thus rendering the particles very hydrophobic. The hydrophobic CaCO_3 precipitates are then filtered by vacuum filtration with a Büchner, washed thoroughly with ethanol and dried at 70°C for 1 hour.

The experiments carried out with soap yielded so hydrophobic particles that, prior to the filtering, they were floating at the surface of the aqueous solution in the blender instead of dropping at the bottom of the vase.

The yield was typically more than 85 % in all cases. .

Characterization:

To identify the crystalline phases, X-ray powder diffraction measurements were performed with a Panalytical Empyrean diffractometer working with the monochromatic CuK α radiation ($\lambda = 1.54 \text{ \AA}$). The X-ray diffraction patterns were recorded from $2\theta = 20^\circ$ to 40° in steps of 0.026° . All the diffraction patterns were analyzed with the MAUD program based on the Rietveld method for refining the atomic fractions and some parameters of each phase [43]. The earlier information on the crystal structures of vaterite [44-47], calcite and aragonite [48] (CIF files) were used as initial inputs to carry out the refinements. As the vaterite structure is still quite controversial we used several variants among which the monoclinic one proposed by Mugnaioli et al. was the most satisfying one [45, 46]. This was the only one able to match the intensities around $2\theta = 38^\circ$. Note that we have fixed the Debye-Waller values since the aim was to identify the phases and since experiments were measured in a limited range of 2θ values. A representation of the structure obtained with VESTA [45] is given in Fig.1.

The Fourier Transform Infrared Spectra (FT-IR) were recorded on a Bruker-vertex 70 V spectrometer with a global light source and a DTGS detector. The spectra were measured in the Attenuated Total Reflectance (ATR) mode using a diamond crystal. The FTIR spectra were recorded in the range of 400 to 4000 cm^{-1} with a resolution of 2 cm^{-1} using 20 scans. For clarity, in the interpretation of I.R. data spectra, we report in Table.I the characteristic vibration bands for the different polymorphs of CaCO_3 and esters of olive oil.

The morphology of particles was imaged by the JEOL JSM 65 VL scanning electron microscope operating at 10 kV with a working distance varying from 9mm to 13mm and a secondary electron detector. S.E.M. Images are analyzed using a method described by M. Almesseire et al. and A.V. Trukanov et al [49-50] where the surface of the particles is used to define an average particle length. Note that vaterite particles are ellipsoidal in shape so that for each particle measurable in the S.E.M. image we have determined its surface S_p using imageJ [49-54]. The average length of the particle was calculated using the equivalent disk diameter by the following equation :

$$\langle d \rangle = 2 \sqrt{\frac{S_t}{\pi}} \quad (4)$$

We are aware that this information is not very precise as we observe only a projection of the particles on the surface of the microscope grid. Yet it gives anstochastic indication of the particle size.

The specific surface area (SSA) value of 1g of CaCO_3 was calculated from the following equation [49-54]:

$$\text{SSA} = \frac{(p_1 S_1 + p_2 S_2 + p_3 S_3 + \dots + p_i S_i)}{100} \quad (5)$$

where p_i is the fraction content (%), S_i is the surface area of particles of given fraction which was calculated as:

$$S_i = \frac{6}{\rho \cdot d_i} \quad (6)$$

d_i is the size (equivalent disk diameter) of a given particle as described in equation (4). The density (ρ) of CaCO_3 was taken equal to the one of vaterite, i.e. 2650 kg/m^3 [55].

For aragonite which exhibits a very different morphology consisting of rodlike bundles we have only measured the average length of bundles as it was too difficult to isolate specific independent rods.

Wettability measurements:

The water and oil contact angles were measured using Attension® - Theta Flex instrument. The contact angle measurements were performed by placing water and oil droplets on powdered samples using a syringe dispersing a controlled volume ($4.5 \mu\text{L}$) of liquid at the surface of the sample. The powdered samples were prepared by filling the groove with an aluminum holder with compacted CaCO_3 powder.

Results and discussion:

Effect of the temperature on the morphology of CaCO_3 particles prepared without hydrophobic coating:

The S.E.M. image of the CaCO_3 particles produced in the absence of soap at two different temperatures (i.e. 30 and 80 °C) are shown in Figure 2. For samples synthesized at 30 °C, the polydisperse egg-shaped aggregates of vaterite can be seen (with dimension varying from 0.5 to 3.5 μm) (Fig. 2a). The histogram of particle size distribution determined from equation 4 is shown in Fig. 2a (mean value is 2.32 μm). The inset in Fig. 2a evidences that rhombohedral shaped particles characteristic of calcite are statistically present in very small quantity. Band assignment for FT-IR of CaCO_3 polymorphs is well established. These absorption bands correspond to symmetric C-O stretching mode (ν_1), CO_3^{2-} out-of-plane bending mode (ν_2), doubly degenerated

asymmetric C-O stretching mode (ν_3) and doubly degenerated in-plane OCO deformation bending mode (ν_4) (see Table. I). As shown in the FTIR spectra in Fig. 3a, the characteristic absorption bands of vaterite near ν_4 at 745, ν_2 at 876, ν_1 at 1089, ν_3 at 1465 cm^{-1} and calcite absorption bands can be observed, but only bands of ν_4 at 848 cm^{-1} [30,41,42, 66-68].

Powder diffraction analysis coupled to Rietveld analysis is a powerful tool to evidence the structure and the phase content of a pulverulent material [43,44,69]. The quantitative XRD analysis clearly indicates the presence of vaterite with a percentage of 98 % and calcite with a percentage of 2 % at 30 °C, as shown in Fig. 4a and Table S1 in Supplementary Information. The Bragg reflections of vaterite are quite broad with full width at half maximum of the order of 0.4°. This is signing the fact that particles of vaterite are made of agglomerated nanograins having a typical size of about 47.8 (9) nm obtained from the fits to the data using the MAUD program.

When the synthesis temperature was increased to 80 °C, the morphology evidenced by SEM changed from spheroidal particles to rod-like particles characteristic of aragonite having several μm in length (Fig. 2b). Some of these particles were agglomerated into bundles. FT-IR experiments carried out on the sample prepared at 80 °C shows the characteristic bands of aragonite located at 713, 856, 1082 and 1475 cm^{-1} corresponding to the ν_4 , ν_2 , ν_1 and ν_3 vibrational modes. Faint humps characteristic of calcite ν_2 , were also observed at 848 cm^{-1} and 876 cm^{-1} in the foot of the strongest absorption band of aragonite ν_2 located at 856 cm^{-1} (see Fig. 3b). The XRD refinement gives a volume fraction of 98 % for aragonite and about 2 % of calcite showing that vaterite has completely disappeared (Fig. 4b; see S. I Table T1). The Bragg peaks are a bit narrower indicating that the particles synthesized at this temperature are bigger. Typical values obtained from the analysis with MAUD gave a particle size of about 52.3 (9) nm. The observation of aragonite at this temperature is definitely expected from previous studies on the precipitation of CaCO_3 . In particular, Ogino et al. have clearly shown that aragonite is predominantly formed above 60°C [70]. These results were confirmed in a recent paper by Cherkas et al. in their study of the stability of CaCO_3 immersed in water at different temperature [71]. Temperature therefore has a decisive effect on the nucleation rate, the growth grain and the final grain morphology. In all cases, the percentage of aragonite increases with increasing temperature. This suggests that vaterite which kinetically forms at the start of the reaction can transform into aragonite at temperatures ≥ 60 °C [71].

With soap at 30°C:

The SEM images of the precipitates prepared at 30 °C in the presence of soap (0.05 g, 0.1 g, 0.2 g, 0.4 g) show particles of vaterite aggregates having an egg shape with, in a few cases, some particles having exotic donuts or flower like shapes (see insets). The usual rhombohedral morphology of calcite was observed very rarely signifying the predominance of vaterite in all samples (image b, Fig. 5). The particles were polydisperse in size ranging from about 1 to 4.5 μm . The mean value determined from equation 4 was found to be $2.70 \pm 0.76 \mu\text{m}$ (Fig. 5).

The FT-IR spectra of these samples confirm the existence of vaterite with absorption peaks located at 745 (ν_4), 876 (ν_2) and 1089 cm^{-1} (ν_1) (see Fig. 6 (left panel) and Table I). The negligible presence of calcite is confirmed by the observation of a single very weak characteristic peak located at 848 cm^{-1} (See Fig. 6 (left panel)).

The IR spectra of pure soap and olive oil are given in S.I. (Fig. S1). The absorption bands located at 2920 and 2954 cm^{-1} shown in Fig.6 are attributed to the oleate alkyl groups (asymmetric and symmetric stretching modes of the H-C-H, respectively), confirming the presence of the soap on the surface of nano- CaCO_3 . They are quite similar whatever the content of soap (0.05, 0.1, 0.2 and 0.4 g).

The X-ray diffraction patterns of these samples confirmed that the 104 characteristic Bragg peak of calcite located at 29.40° was almost invisible (Fig.6 (right panel)). The quantitative Rietveld analysis shows that vaterite reaches a volume fraction bigger or equal to 99 %, in all cases, the remaining traces being attributed to calcite (See S.I. Table T1). No trace of aragonite was detected.

Fig. 5 also shows the size distributions of vaterite obtained by statistical analyzes of SEM images. Its specific surface area (SSA) was calculated using equation (5). It is well known that the SSA is closely related to the size of the particles. In this case we found that the particle size was almost constant except for a slight increase of the average diameter for particles prepared with soap. In that case the standard deviation was found to be bigger than for pure vaterite particles. We found that the surface area was (25.2 m^2/g) for pure vaterite. In the presence of soap, the SSA of vaterite was calculated to be 22.1 m^2/g for 0.05g, 20.9 m^2/g for 0.1g, 20.2 m^2/g for 0.2g and 20.1 m^2/g for 0.4g. We consider that the observed decrease of the SSA is here related to the very polydispersity of the selected particles with a bigger number of small particles.

With soap at 80°C :

At 80 °C (see Fig. 7/ a; b; c; d), the aragonite particles having a rod like shape with a length ranging from 2 to 9 μm were formed. Vaterite and calcite were respectively observed next to the rods (Fig. 7). The FTIR measurements show absorption bands located at 1082 (ν_1), 756 (ν_2), 713 (ν_4) and 700 cm^{-1} (ν_4) corresponding to aragonite (Fig. 8 (left panel) and Table. I). Peaks at wave numbers of 2920 and 2954 cm^{-1} originate from the symmetric stretching vibration (H-C-H) of the alkyl chain of soap and confirm the successful presence of soap at the surface of CaCO_3 particles Fig. S1 (S.1). The intensity of the soap peaks was quite similar whatever the soap quantity (i.e 0.05 , 0.1 , 0.2 and 0.4 g). The Rietveld refinement of the X-ray patterns indicates that the volume fraction decreases from 97 to 95, 90 and 75 % for aragonite when the soap content increases, while calcite is present with a maximum amount of 1 % (in the specific case of T= 80 °C with 0.1 g of soap). For low amount of soap, vaterite is slightly visible in the X-ray powder diffraction patterns while it is observed with greater contents for 0.2 g and 0.4 g. The vaterite fraction increases from 3 % to 24 % at the highest concentration of soap (See S.I Table T1; Fig. 8 (right panel)). It thus appears that soap favors the formation of vaterite and reduces the content of aragonite. During the soap preparation, glycerol is released. Glycerol is known to stabilize vaterite and this could explain why the amount of vaterite is positively correlated to the amount of soap [16, 72]. These results are in good agreement with the results obtained by IR and SEM measurements.

Water contact angle:

The evolution of the water and oil contact angles as a function of the added mass of soap at 30 °C and 80 °C is shown in Figure 9. For both temperatures, the water contact angle increases with added masses of soap from a fully wetted state (i.e. = 0°) to a superhydrophobic state (i.e. > 150°) [73]. The highest value of the contact angle was obtained for aragonite CaCO_3 particles prepared at 80 °C with 0.4g of soap. For a given mass of soap, one can note that the measured water contact angle is always higher for aragonite particles (T=80 °C) than for vaterite ones (T=30 °C). A possible explanation can be found in the highly different morphology of these particles. As seen in the S.E.M. images, vaterite crystallizes in spheroidal particles while aragonite exhibits a rod like shape. It is thus possible that the morphology of aragonite produces a rougher surface that would favor a higher contact angle. The effect would be similar to the one observed on lotus leaves or on flat and patterned

surfaces[74]. The similar experiments were carried out with oil. Without soap, one can clearly see that oil has a better wettability for aragonite than for vaterite. Aragonite particles prepared at $T=80\text{ }^{\circ}\text{C}$ show a higher oleophilic property (contact angle close to 65°) than vaterite ones prepared at $T=30\text{ }^{\circ}\text{C}$ (contact angle close to 82°). In the presence of soap, the contact angle of olive oil with hydrophobic CaCO_3 becomes equal to zero for both aragonite and vaterite. This confirms that these particles are oleophilic.

Selective oil absorption:

The hydrophobic CaCO_3 particles have a very high contact angle with water unlike the very low contact angle with oils, which makes them a selective absorbent of oils spilled on water. For this purpose, the sample prepared at 80°C with soap (0.4g) was placed in a pouch that was immersed in a mixture containing olive oil and water. As shown in Fig. 10, we notice that CaCO_3 functionalized with soap rejects water and selectively retains oils. This can be explained as follows: the incorporation of carboxylates (coming from olive oil) gives a strong increase in the content of Ca-oleate which has an hydrophilic head and an hydrophobic aliphatic tail. The presence of hydrophobic tails at the surface of CaCO_3 makes the CaCO_3 particles oleophilic as evidenced by the oil contact angle ($\Theta=0$). Oil can thus be recovered by binding to the oleophilic part of the CaCO_3 [38].

With the aim of reducing the different levels of environmental pollution generated by mineral oils such as cooking oil and motor oil, CaCO_3 hydrophobic powder can be used as a good anti-pollution absorbent to clean up dispersion in water. In order to measure the absorption capacity, three experiments were conducted in which 3g of superhydrophobic aragonite powder was placed in a pouch. The amount of oil that was dispersed on the surface of water increased from one experiment to the next going from 0.5 g to 1 g and finally 2 g. The adsorption of oil was occurring within less than a few minutes likely at the surface of particles rather than in the bulk. For 0.5 g, the particles quickly adsorbed the oil in about one minute. For 1g, the adsorption took more time compared to 0.5 g (approximately 3 min). When the oil mass was increased to 2 g, the adsorption time also increased to about 6 min. This increase was attributed to the fact that the adsorption capacity was becoming more saturated. The final weight measured after adsorption was 3.5, 4 and 4.6 g. This was showing that the amount of olive oil that could be recovered at the surface of water was at maximum of 1.6g of oil for 3g of powder, i.e. a bit more than 50%. This value is far less than the one achieved by Sarkar et Mahapatra [38]

using immobilized superhydrophobic calcium carbonate particles in polyurethane foams. The reason is likely related to a different oil (diesel instead of olive oil) and to the use of a foam instead of a pouch.

In previous studies, hydrophobic particles were usually made with oleic acid ($C_{17}H_{33}COOH$) mixed in a $CaCl_2$ solution [36, 75]. In fact, in basic condition oleic acid transforms into sodium oleate which, in turn, can react with Ca^{2+} ions to form Ca-oleate [38]. This indicates that Ca^{2+} ions are more chemically active than Na^+ ions to bind carboxylate ions. This was recently evidenced by D. Mendes de Oliveira et al [73]. As shown by Wang et al, increasing the concentration of oleic acid obviously reduced the wettability of $CaCO_3$ and therefore increased the relative contact angle. This indicates that oleic acid induces hydrophobicity to $CaCO_3$ [36, 37, 76]. In addition, oleic acid not only affects the transformation of hydrophilic $CaCO_3$ particles into hydrophobic ones but also causes changes in its morphology [38]. However, oleic acid is extremely expensive and cost-effective synthesis of hydrophobic $CaCO_3$ particles cannot be achieved with oleic acid on a large scale. This is why we have been using in this work olive oil which mainly contains esters of oleic, linoleic and palmitic acids. Olive oil is available in very large quantities at a cheap price and is therefore quite attractive. In addition, it is biocompatible. In 2019, a production of 3.67 million tons of olive oil was estimated by the international olive oil council [77].

In saponification, sodium carboxylates and in particular sodium oleate ($NaC_{17}H_{33}COO$), sodium linoleate and sodium palmitate are formed together with the release of glycerol ($HOH_2C-CHOH-CH_2OH$). When mixing with the precursors of $CaCO_3$, carbonate CO_3^{2-} and calcium Ca^{2+} ions are available in the $CaCl_2$ and $NaCO_3$ solutions. The carboxylates have a hydrophobic carbon chain and a hydrophilic head. The hydrophilic carboxylic head can link to Ca^{2+} inwards while the hydrophobic chain points outwards. We anticipate that soap molecules are covering the surface of $CaCO_3$ via the formation of calcium carboxylates (and particularly calcium oleate $C_{17}H_{33}COOCa$) rather than in the core of the particles. This statement agrees with the fact that the hydrophobic particles are floating at the surface of water [36, 78]. In addition, the release of glycerol in the soap during the saponification of olive oil is certainly promoting the stabilization of vaterite, as evidenced in the 0.4g sample, where vaterite is observed at 80 °C coexisting with aragonite [16, 70]. In absence of soap, we never see vaterite forming at this temperature.

Conclusion:

In summary, we have shown that hydrophilic CaCO_3 can be turned into hydrophobic particles using cost-effective ingredients like olive oil and baking soda. This study is based on the saponification of olive oil into hydrophobic solid soap using olive oil and sodium hydroxide. The esters contained in olive oil are transformed into carboxylates. The hydrophobic particles of CaCO_3 are produced by the co-precipitation process at 30 °C and 80 °C using various concentrations of soap incorporated into the aqueous medium as an additive. Without soap, the contact angle is zero, a sign of the original hydrophilic nature of CaCO_3 . The contact angles after adding soap were positively correlated with the amount of soap added. At 0.4 g of soap, the contact angles with water reach a maximum of 174° and 163°, respectively, for aragonite and vaterite. The hydrophobicity arises from the aliphatic carbon chain of soap carboxylates.

The hydrophobic character of the particles was an advantage to demonstrate the absorbency of oil on the surface of water. The use of natural products such as olive oil and baking soda are definitely a novel route using green chemistry to reduce the cost of manufacturing these superhydrophobic particles.

Acknowledgements:

The authors gratefully acknowledge Mr Anthony ROUSSEAU for his help in S.E.M. experiments. They thank T. Beuvier and O. Cherkas for useful discussions.

References:

1. Saraya, M.E.-S.I. and H.-L. Rokbaa, *Formation and Stabilization of Vaterite Calcium Carbonate by Using Natural Polysaccharide*. Adv. Nanopart, 2017. **6**: p. 158-162.
2. Chen, J. and L. Xiang, *Controllable synthesis of calcium carbonate polymorphs at different temperatures*. Powder technology, 2009. **189**(1): p. 64-69.
3. Handayani, M., et al. *Synthesis of Calcite Nano Particles from Natural Limestone assisted with Ultrasonic Technique*. in *IOP Conference Series: Materials Science and Engineering*. 2018. IOP Publishing.
4. Gopi, S., V. Subramanian, and K. Palanisamy, *Aragonite–calcite–vaterite: A temperature influenced sequential polymorphic transformation of CaCO₃ in the presence of DTPA*. Materials Research Bulletin, 2013. **48**(5): p. 1906-1912.
5. Kontoyannis, C.G. and N.V. Vagenas, *Calcium carbonate phase analysis using XRD and FT-Raman spectroscopy*. Analyst, 2000. **125**(2): p. 251-255.
6. Seo, K.-S., et al., *Synthesis of calcium carbonate in a pure ethanol and aqueous ethanol solution as the solvent*. Journal of crystal growth, 2005. **276**(3-4): p. 680-687.
7. Hadiko, G., et al., *Synthesis of hollow calcium carbonate particles by the bubble templating method*. Materials Letters, 2005. **59**(19-20): p. 2519-2522.
8. Tao, L., et al., *CO₂ capture and separation on charge-modulated calcite*. Applied Surface Science, 2020. **530**: p. 147265.
9. Tan, G.-L., et al., *Structures, morphological control, and antibacterial performance of tungsten oxide thin films*. Ceramics International, 2021. **47**(12): p. 17153-17160.
10. Tao, L., et al., *Flue Gas Separation at Organic-Inorganic Interface under Geological Conditions*. Surfaces and Interfaces, 2021: p. 101462.
11. Macías-Sánchez, E., et al., *Transformation of ACC into aragonite and the origin of the nanogranular structure of nacre*. Scientific reports, 2017. **7**(1): p. 1-11.
12. Jackson, A., J.F. Vincent, and R. Turner, *The mechanical design of nacre*. Proceedings of the Royal society of London. Series B. Biological sciences, 1988. **234**(1277): p. 415-440.

13. Achour, A., et al., *Synthesis and characterization of porous CaCO₃ micro/nano-particles*. The European Physical Journal Plus, 2017. **132**(6): p. 267.
14. Rong, X., et al., *Controllable Synthesis of Calcium Carbonate with Different Morphologies and Phases Assisted by F127*. Asian Journal of Chemistry, 2014. **26**(13): p. 3971.
15. Pérez-Villarejo, L., et al., *Synthesis of vaterite CaCO₃ as submicron and nanosized particles using inorganic precursors and sucrose in aqueous medium*. Ceramics International, 2018. **44**(5): p. 5291-5296.
16. Konopacka-Łyskawa, D., *Synthesis methods and favorable conditions for spherical vaterite precipitation: a review*. Crystals, 2019. **9**(4): p. 223.
17. Wu, Z.G., et al., *Preparation of vaterite CaCO₃ microspheres by fast precipitation method*. International Journal of Materials Research, 2017. **108**(3): p. 245-248.
18. Ramesh, T., S. Inchara, and K. Pallavi, *Para-amino benzoic acid-mediated synthesis of vaterite phase of calcium carbonate*. Journal of Chemical Sciences, 2015. **127**(5): p. 843-848.
19. Guo, X., et al., *Controlled crystallization of hierarchical and porous calcium carbonate crystals using polypeptide type block copolymer as crystal growth modifier in a mixed solution*. CrystEngComm, 2011. **13**(6): p. 2054-2061.
20. Ševčík, R., et al., *Characterization of vaterite synthesized at various temperatures and stirring velocities without use of additives*. Powder Technology, 2015. **284**: p. 265-271.
21. Cherkas, O., et al., *On the kinetics of phase transformations of dried porous vaterite particles immersed in deionized and tap water*. Advanced Powder Technology, 2018. **29**(11): p. 2872-2880.6. 7.
8. 9. 10. 11. 12. 13. 14. 15. 16.
22. Beuquier, T., et al., *Synthesis of hollow vaterite CaCO₃ microspheres in supercritical carbon dioxide medium*. Journal of Materials Chemistry, 2011. **21**(26): p. 9757-9761.
23. Zhao, D., et al., *Synthesis of template-free hollow vaterite CaCO₃ microspheres in the H₂O/EG system*. Materials Letters, 2013. **104**: p. 28-30.
24. Vikulina, A., et al., *The mechanism of catalase loading into porous vaterite CaCO₃ crystals by co-synthesis*. Physical Chemistry Chemical Physics, 2018. **20**(13): p. 8822-8831.

25. Kim, B.-J., et al., *Synthesis of CaCO₃ using CO₂ at room temperature and ambient pressure*. Materials Letters, 2017. **190**: p. 45-47.
26. Park, J.-H. and S.-G. Oh, *Preparation of CaO as OLED getter material through control of crystal growth of CaCO₃ by block copolymers in aqueous solution*. Materials Research Bulletin, 2009. **44**(1): p. 110-118.
27. Wang, C., et al., *Synthesis and characterization of hydrophobic calcium carbonate particles via a dodecanoic acid inducing process*. Powder Technology, 2010. **198**(1): p. 131-134.
28. Amer, L., et al., *The effect of ergocalciferol on the precipitation of calcium carbonate*. Journal of Crystal Growth, 2018. **501**: p. 49-59.
29. Song, X., et al., *Effect of pH and temperatures on the fast precipitation vaterite particle size and polymorph stability without additives by steamed ammonia liquid waste*. Powder Technology, 2020. **374**: p. 263-273.
30. Kogo, M., et al., *Control of aragonite formation and its crystal shape in CaCl₂-Na₂CO₃-H₂O reaction system*. Journal of Crystal Growth, 2021. **559**: p. 125964.
31. Gopi, S.P. and V.K. Subramanian, *Polymorphism in CaCO₃—Effect of temperature under the influence of EDTA (di sodium salt)*. Desalination, 2012. **297**: p. 38-47.
32. Miyazaki, T., T. Arii, and Y. Shirosaki, *Control of crystalline phase and morphology of calcium carbonate by electrolysis: Effects of current and temperature*. Ceramics International, 2019. **45**(11): p. 14039-14044.
33. Oral, Ç.M. and B. Ercan, *Influence of pH on morphology, size and polymorph of room temperature synthesized calcium carbonate particles*. Powder technology, 2018. **339**: p. 781-788.
34. Tsuzuki, T., K. Pethick, and P.G. McCormick, *Synthesis of CaCO₃ nanoparticles by mechanochemical processing*. Journal of Nanoparticle Research, 2000. **2**(4): p. 375-380.
35. Juhasz-Bortuzzo, J.A., et al., *Sonosynthesis of vaterite-Type calcium carbonate*. Crystal Growth & Design, 2017. **17**(5): p. 2351-2356.
36. Wang, C., et al., *A novel aqueous-phase route to synthesize hydrophobic CaCO₃ particles in situ*. Materials Science and Engineering: C, 2007. **27**(1): p. 42-45.

37. Wang, C., et al., *Synthesis and character of super-hydrophobic CaCO₃ powder in situ*. Powder Technology, 2010. **200**(1-2): p. 84-86.
38. Sarkar, A. and S. Mahapatra, *Novel hydrophobic vaterite particles for oil removal and recovery*. Journal of Materials Chemistry A, 2014. **2**(11): p. 3808-3818.
39. Jiang, J., et al., *Roles of oleic acid during micropore dispersing preparation of nano-calcium carbonate particles*. Applied surface science, 2011. **257**(16): p. 7047-7053.
40. Lee, J., S.H. Jo, and J. Lim, *Effect of surface modification of CaCO₃ nanoparticles by a silane coupling agent methyltrimethoxysilane on the stability of foam and emulsion*. Journal of Industrial and Engineering Chemistry, 2019. **74**: p. 63-70.
41. Boskou, D., G. Blekas, and M. Tsimidou, *Olive oil composition*, in *Olive Oil*, 2006, Elsevier. p. 41-72.35.
42. Rohman, A. and Y. Che Man, *Quantification and classification of corn and sunflower oils as adulterants in olive oil using chemometrics and FTIR spectra*. The Scientific World Journal, 2012
43. Lutterotti, L., S. Matthies, and H. Wenk, *MAUD: a friendly Java program for material analysis using diffraction*. IUCr: Newsletter of the CPD, 1999. **21**(14-15).
44. Le Bail, A., S. Ouhenia, and D. Chateigner, *Microtwinning hypothesis for a more ordered vaterite model*. Powder Diffraction, 2011. **26**(1): p. 16-21.
45. Mugnaioli, E., et al., *Ab initio structure determination of vaterite by automated electron diffraction*. Angewandte Chemie International Edition, 2012. **51**(28): p. 7041-7045.
46. Demichelis, R., et al., *The multiple structures of vaterite*. Crystal growth & design, 2013. **13**(6): p. 2247-2251.
47. Christy, A.G., *A review of the structures of vaterite: the impossible, the possible, and the likely*. Crystalgrowth & design, 2017. **17**(6): p. 3567-3578.
48. Gražulis, S., et al., *Crystallography Open Database—an open-access collection of crystal structures*. Journal of applied crystallography, 2009. **42**(4): p. 726-729.
49. Almessiere, M.A., et al., *Influence of Dy³⁺ Ions on the Microstructures and Magnetic, Electrical, and Microwave Properties of [Ni_{0.4}Cu_{0.2}Zn_{0.4}](Fe_{2-x}Dy_x)O₄ (0.00 ≤ x ≤ 0.04) Spinel Ferrites*. ACS omega, 2021. **6**(15): p. 10266-10280.

50. Trukhanov, A., et al., *Impact of the heat treatment conditions on crystal structure, morphology and magnetic properties evolution in BaM nanohexaferrites*. Journal of Alloys and Compounds, 2021. **866**: p. 158961.
51. Almessiere, M., et al., *Correlation between microstructure parameters and anti-cancer activity of the [Mn_{0.5}Zn_{0.5}](Eu_xNd_xFe_{2-2x})O₄ nanoferrites produced by modified sol-gel and ultrasonic methods*. Ceramics International, 2020. **46**(6): p. 7346-7354.
52. Trukhanov, A., et al., *Influence of the dysprosium ions on structure, magnetic characteristics and origin of the reflection losses in the Ni-Co spinels*. Journal of Alloys and Compounds, 2020. **841**: p. 155667.
53. Almessiere, M., et al., *Microstructure, dielectric and microwave features of [Ni_{0.4}Cu_{0.2}Zn_{0.4}](Fe_{2-x}Tbx)O₄ (x ≤ 0.1) nanospinel ferrites*. Journal of Materials Research and Technology, 2020. **9**(5): p. 10608-10623.
54. Zubar, T., et al., *The effect of heat treatment on the microstructure and mechanical properties of 2D nanostructured Au/NiFe system*. Nanomaterials, 2020. **10**(6): p. 1077.
55. Steciuk, G., et al., *Stacking sequence variations in vaterite resolved by precession electron diffraction tomography using a unified superspace model*. Scientific reports, 2019. **9**(1): p. 1-12.
56. Chen, Z., X. Li, and B. Zheng, *Can Spherical Vaterite Be Biomimetic Synthesized by Using Histidine-Grafted-Chitosan as an Organic Matrix?* Journal of Inorganic and Organometallic Polymers and Materials, 2017. **27**(4): p. 1014-1021.
57. Vagenas, N., A. Gatsouli, and C. Kontoyannis, *Quantitative analysis of synthetic calcium carbonate polymorphs using FT-IR spectroscopy*. Talanta, 2003. **59**(4): p. 831-836.
58. Gunasekaran, S., G. Anbalagan, and S. Pandi, *Raman and infrared spectra of carbonates of calcite structure*. Journal of Raman Spectroscopy: An International Journal for Original Work in all Aspects of Raman Spectroscopy, Including Higher Order Processes, and also Brillouin and Rayleigh Scattering, 2006. **37**(9): p. 892-899.
59. Xu, B. and K.M. Poduska, *Linking crystal structure with temperature-sensitive vibrational modes in calcium carbonate minerals*. Physical Chemistry Chemical Physics, 2014. **16**(33): p. 17634-17639.
60. Wang, F., et al., *Green synthesis and bioactivity of vaterite-doped beta-dicalcium silicate bone cement*. Ceramics International, 2016. **42**(1): p. 1856-1861.

61. Xie, A.-J., et al., *Crystal growth of calcium carbonate with various morphologies in different amino acid systems*. Journal of Crystal Growth, 2005. **285**(3): p. 436-443.
62. Lerma-García, M., et al., *Authentication of extra virgin olive oils by Fourier-transform infrared spectroscopy*. Food Chemistry, 2010. **118**(1): p. 78-83.
63. Gurdeniz, G., F. Tokatli, and B. Ozen, *Differentiation of mixtures of monovarietal olive oils by mid-infrared spectroscopy and chemometrics*. European Journal of Lipid Science and Technology, 2007. **109**(12): p. 1194-1202.
64. Rohman, A., Y.C. Man, and F.M. Yusof, *The use of FTIR spectroscopy and chemometrics for rapid authentication of extra virgin olive oil*. Journal of the American Oil Chemists' Society, 2014. **91**(2): p. 207-213.
65. Rohman, A. and Y.B.C. Man, *Determination of sodium fatty acid in soap formulation using Fourier Transform Infrared (FTIR) spectroscopy and multivariate calibrations*. Journal of Surfactants and Detergents, 2011. **14**(1): p. 9-14.
66. Altaf, F., et al., *Synthesis and electrochemical investigations of ABPBI grafted montmorillonite based polymer electrolyte membranes for PEMFC applications*. Renewable Energy, 2021. **164**: p. 709-728.
67. Zhang, M., et al., *Greatly enhanced dielectric charge storage capabilities of layered polymer composites incorporated with low loading fractions of ultrathin amorphous iron phosphate nanosheets*. Journal of Materials Chemistry C, 2021. **9**(32): p. 10414-10424.
68. Sun, L., et al., *Asymmetric Trilayer All-Polymer Dielectric Composites with Simultaneous High Efficiency and High Energy Density: A Novel Design Targeting for Advanced Energy Storage Capacitors*. Advanced Functional Materials, 2021: p. 2100280.
69. Shan, K., et al., *Mixed conductivity and the conduction mechanism of the orthorhombic CaZrO₃ based materials*. Surfaces and Interfaces, 2021. **23**: p. 100905.
70. Ogino, T., T. Suzuki, and K. Sawada, *The formation and transformation mechanism of calcium carbonate in water*. Geochimica et Cosmochimica Acta, 1987. **51**(10): p. 2757-2767.
71. Cherkas, O., et al., *On the kinetics of phase transformations of dried porous vaterite particles immersed in deionized and tap water*. Advanced Powder Technology, 2018. **29**(11): p. 2872-2880.

72. Li, Q., et al., *Solvothermal growth of vaterite in the presence of ethylene glycol, 1, 2-propanediol and glycerin*. Journal of crystal growth, 2002. **236**(1-3): p. 357-362.
73. Wang, S. and L. Jiang, *Definition of superhydrophobic states*. 2007.
74. Jung, Y. and B. Bhushan, *Wetting behaviour during evaporation and condensation of water microdroplets on superhydrophobic patterned surfaces*. Journal of microscopy, 2008. **229**(1): p. 127-140.
75. Mendes de Oliverira, D. et al., *Binding of divalent cations to acetate: molecular simulations guided by Raman spectroscopy*, *Phys. Chem. Chem. Phys.*, 2020. **22**: p. 24014-24027.
76. Wang, C., et al., *Biomimetic nucleation and growth of hydrophobic vaterite nanoparticles with oleic acid in a methanol solution*. Applied surface science, 2007. **253**(10): p. 4768-4772.
77. Barranco, D., et al., *World catalogue of olive varieties*. International Olive Oil Council, Madrid, 2000. **360**.
78. Wang, C., et al., *Biomimetic synthesis of hydrophobic calcium carbonate nanoparticles via a carbonation route*. Powder technology, 2006. **170**(1): p. 31-35.

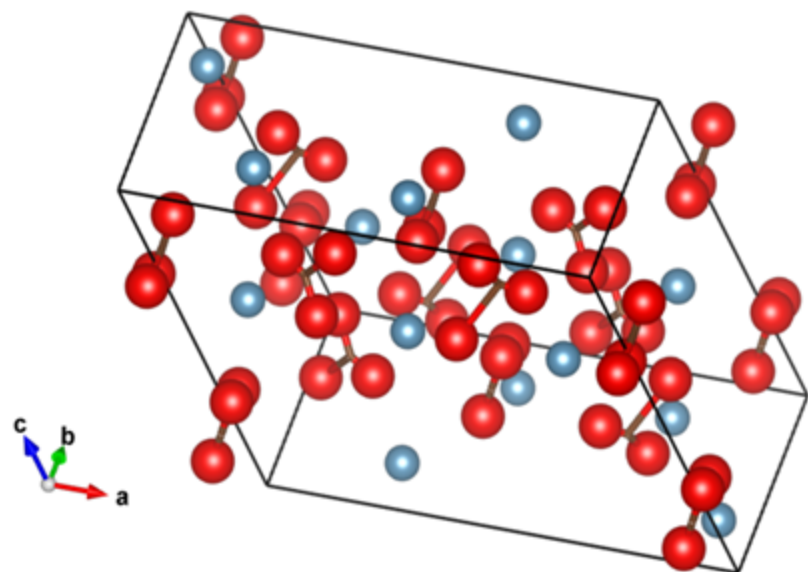


Figure.1: The monoclinic structure of vaterite suggested by Mugnaioli et al (Carbon atoms are omitted for clarity; oxygen ions are in red and calcium ions in blue).

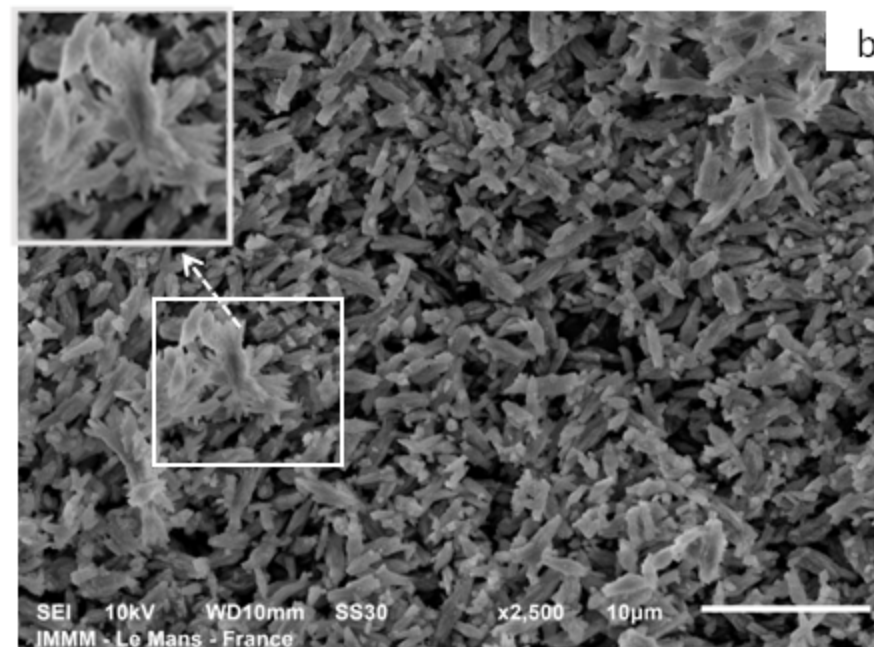
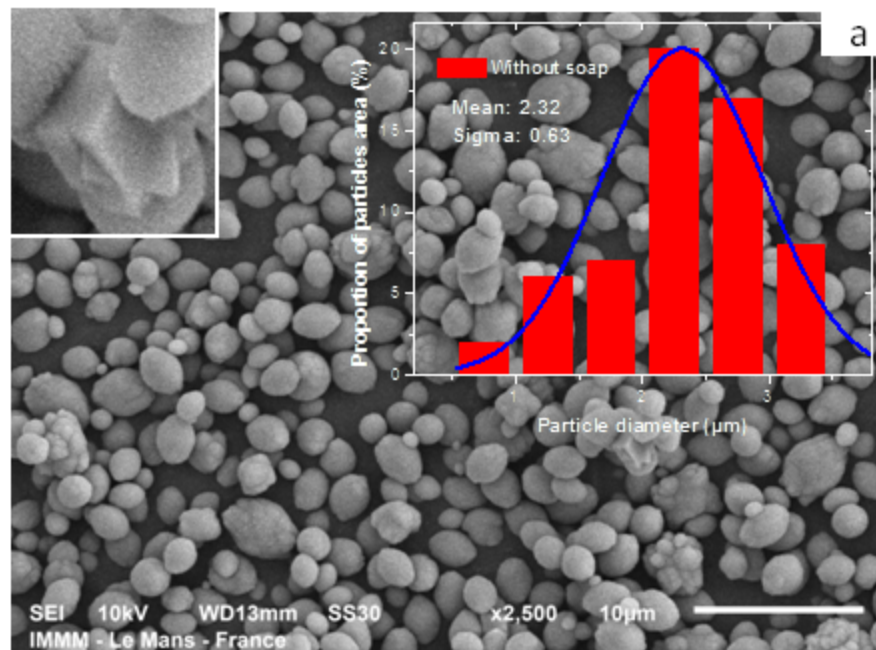


Fig.2: SEM images and histogram of size distribution of the particles produced:
 (a) sample at 30 °C without soap; (b) 80 °C without soap.

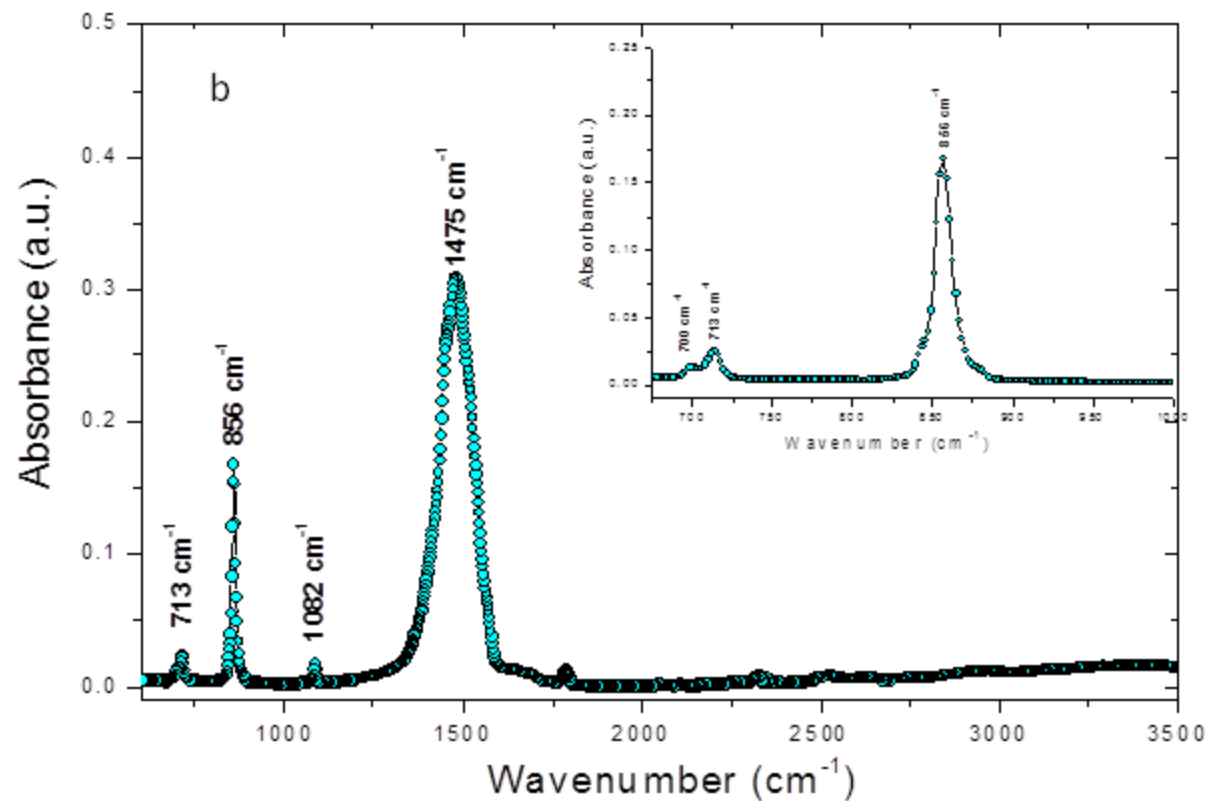
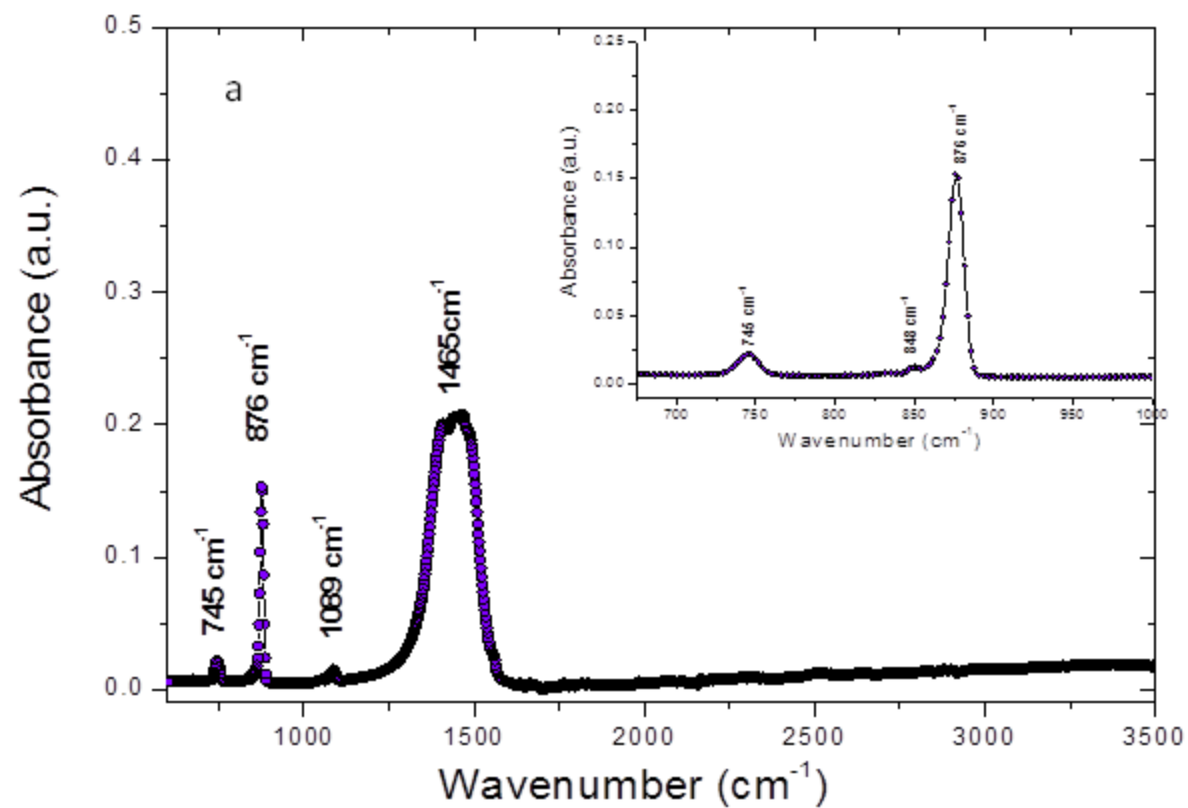


Fig.3 : FT-IR spectrum of CaCO_3 particles nucleated without soap :
 (a) at 30°C ; (b) at 80°C . Arrows are lines indicating the presence of a very small amount of calcite in both samples

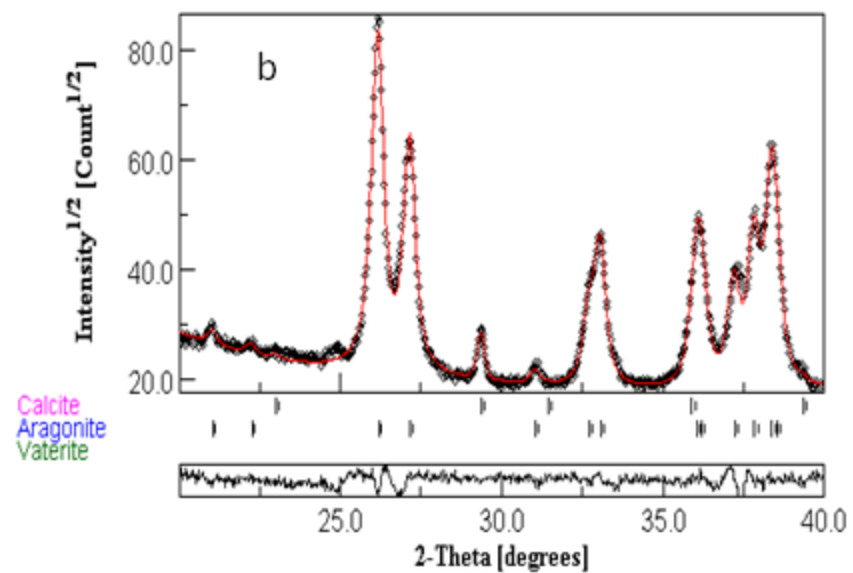
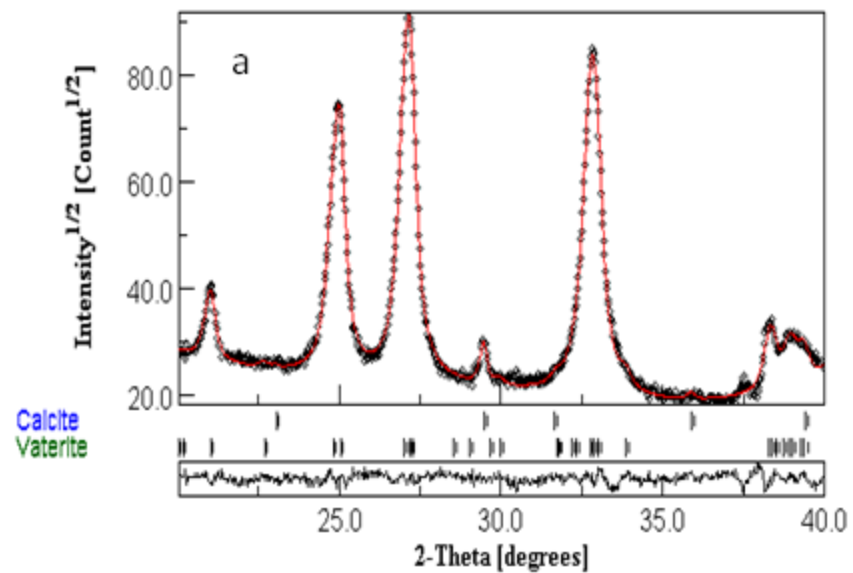


Fig.4 : Observed, calculated and difference curves deduced from the Rietveld analysis :
 (a) sample at 30 °C without soap; (b) 80 °C without soap.

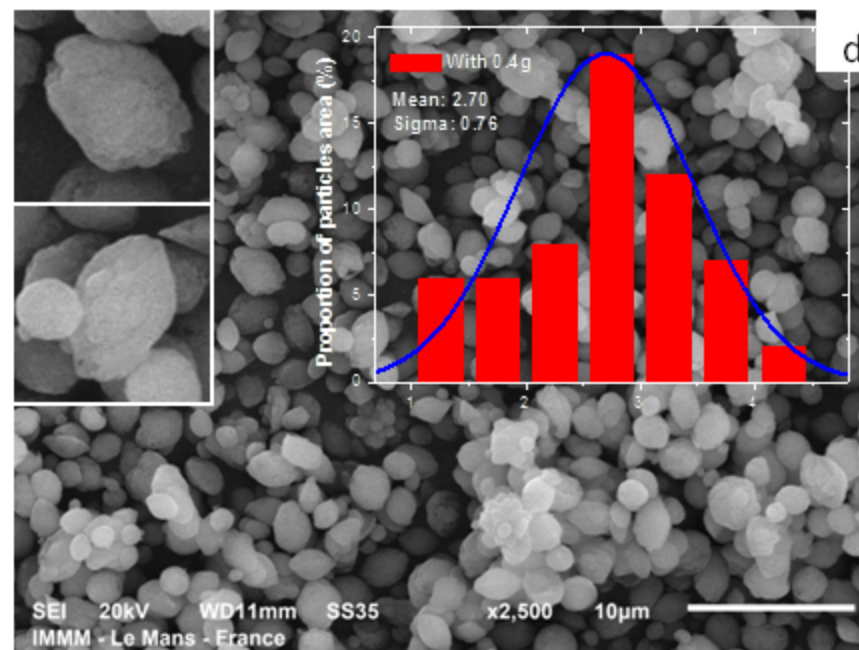
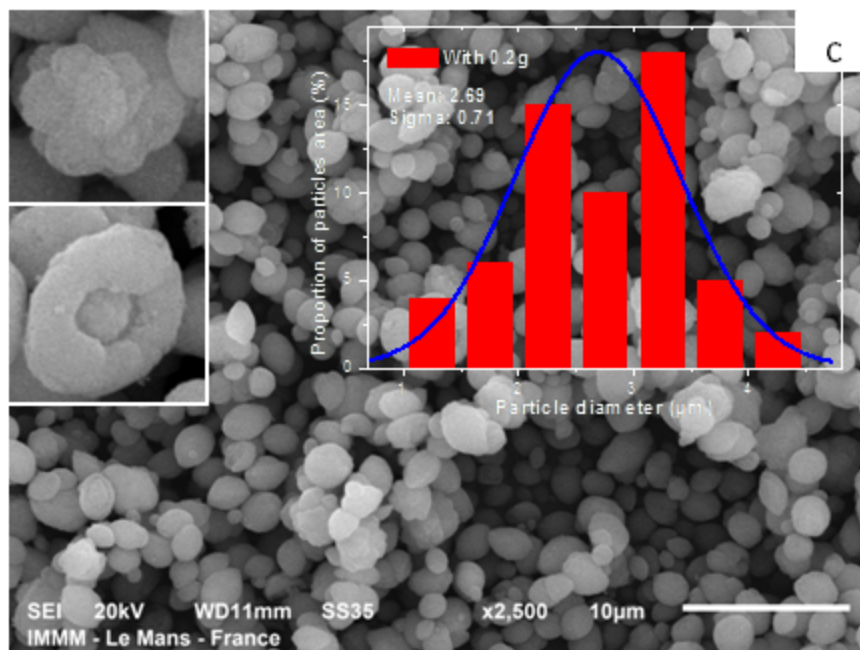
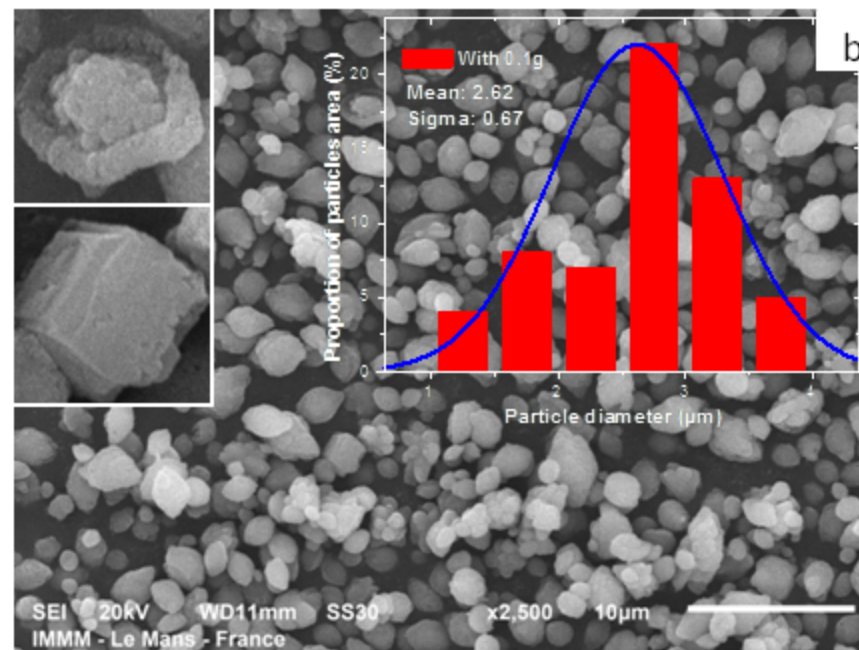
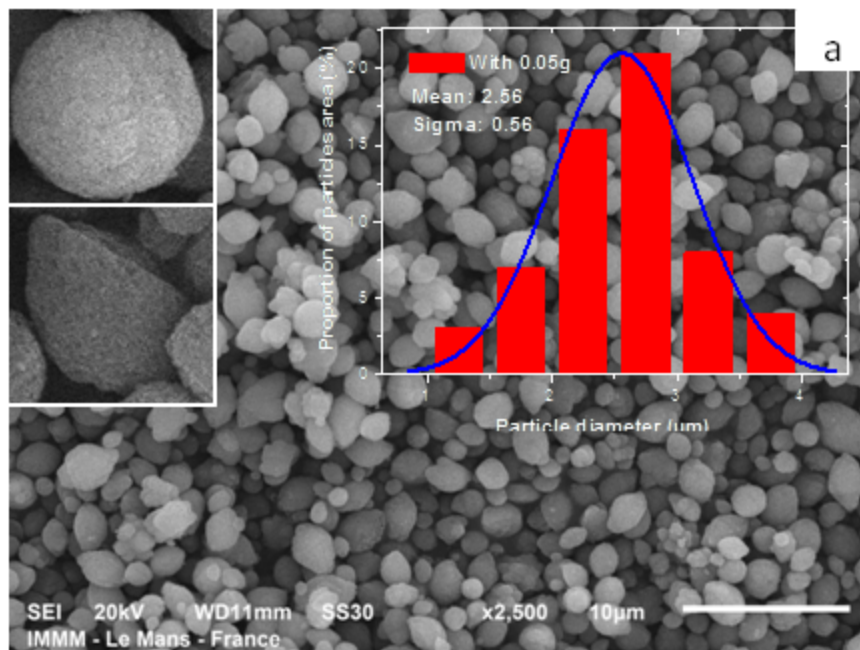


Fig.5 : SEM images and histograms of size distribution :
 (a) sample with 0.05 g soap ; (b) with 0.1 g soap ; (c) with 0.2 g soap ; (d) with 0.4 g.

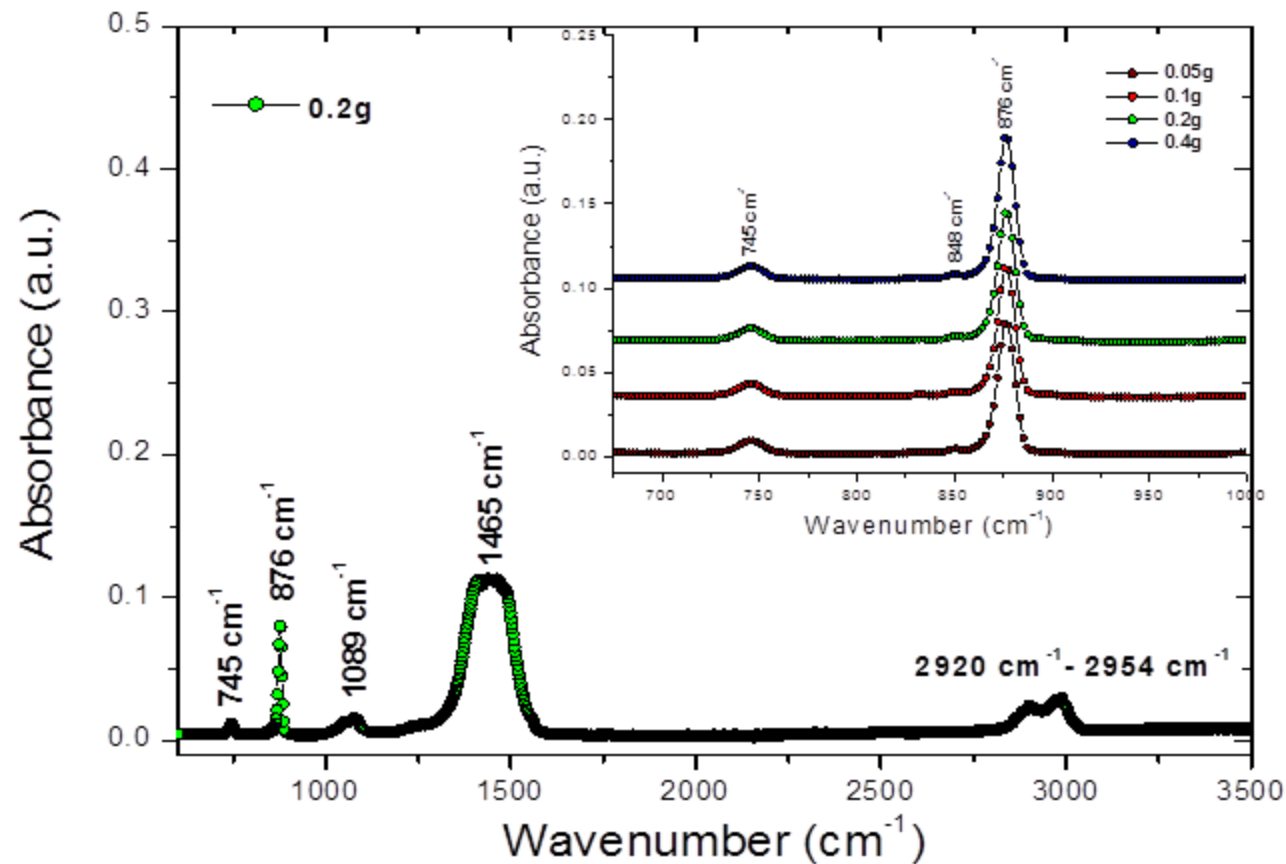
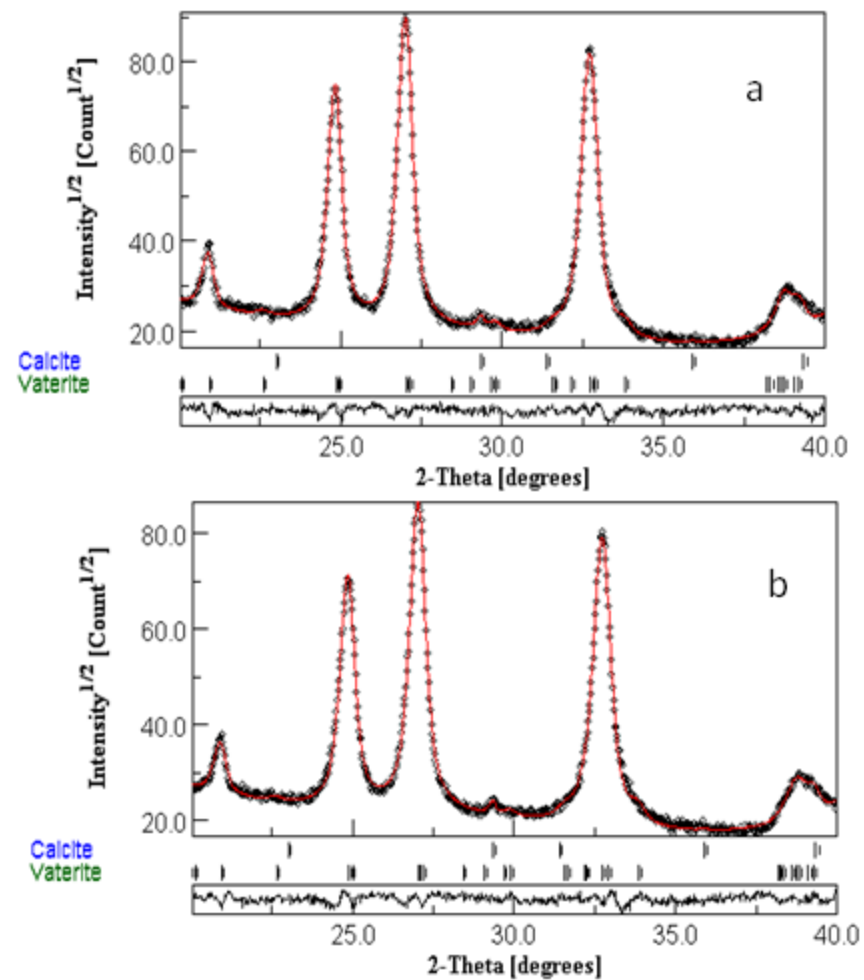


Fig.6 :

Left: FT-IR spectrum of CaCO_3 particles nucleated with soap :
0.05g, 0.1g, 0.2g, 0.4g at 30°C.

Right: Observed, calculated and difference curves after Rietveld refinement :
(a) 30 °C with 0.2 g soap ; (b) 30 °C with 0.4 g soap.



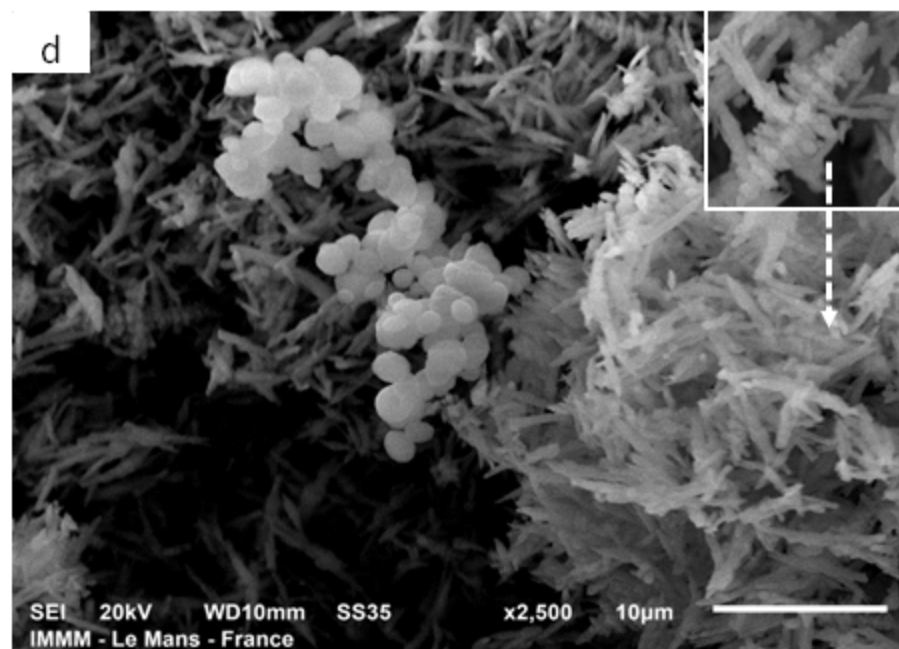
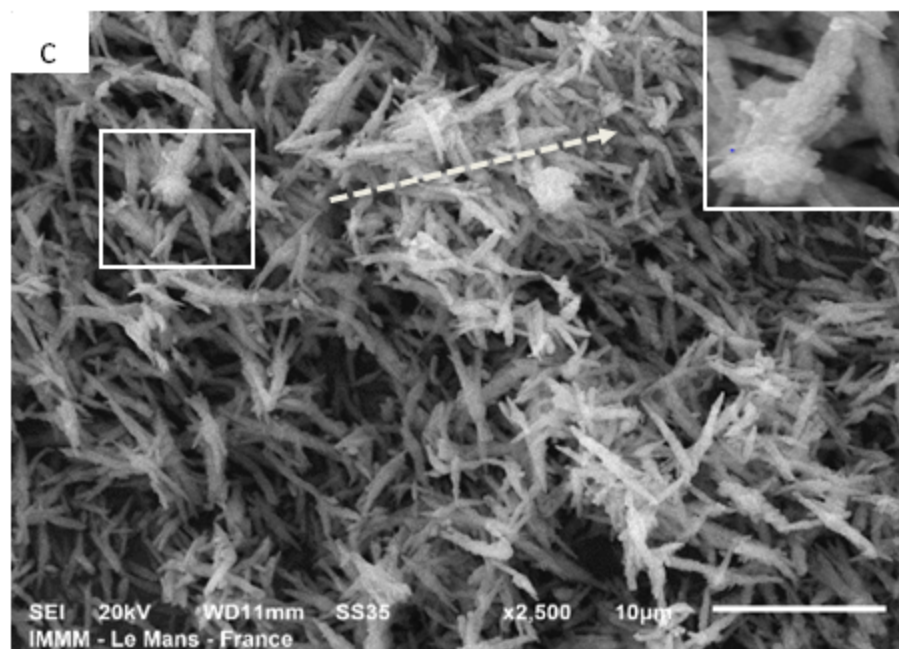
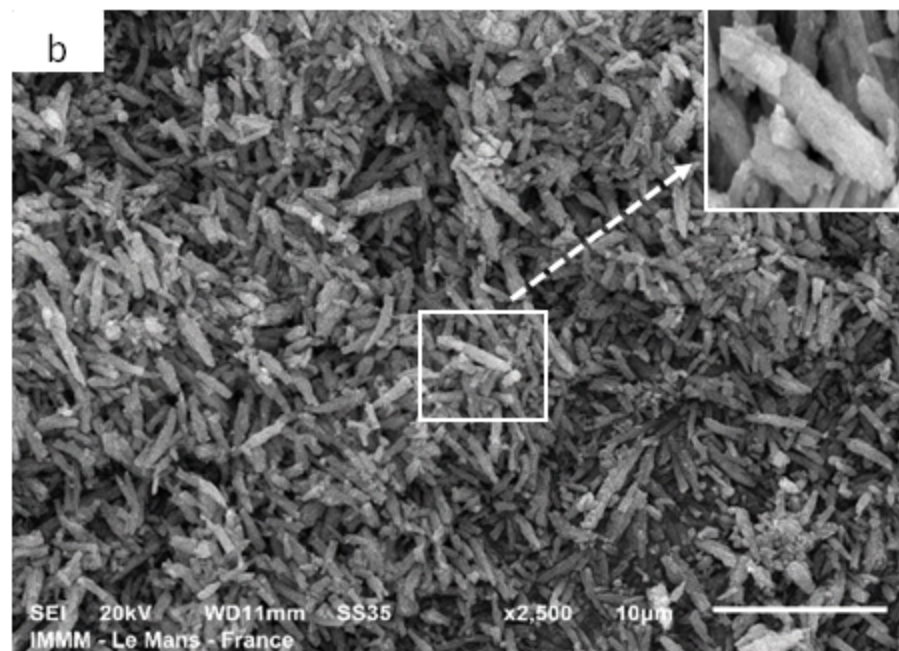
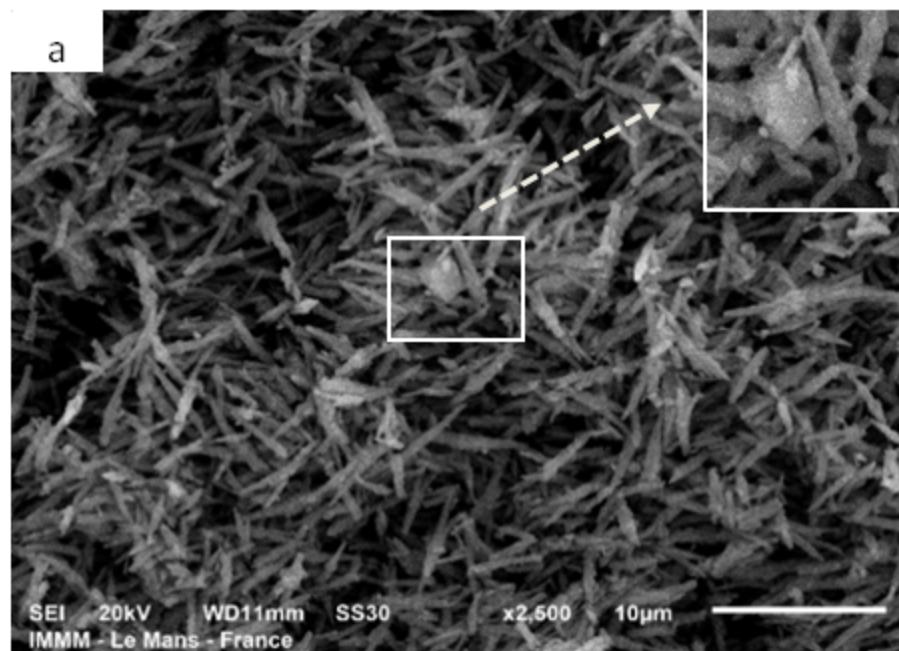


Fig.7: SEM images:

(a) sample with 0.05 g soap ; (b) with 0.1 g soap ; (c) with 0.2 g soap ; (d) with 0.4 g.

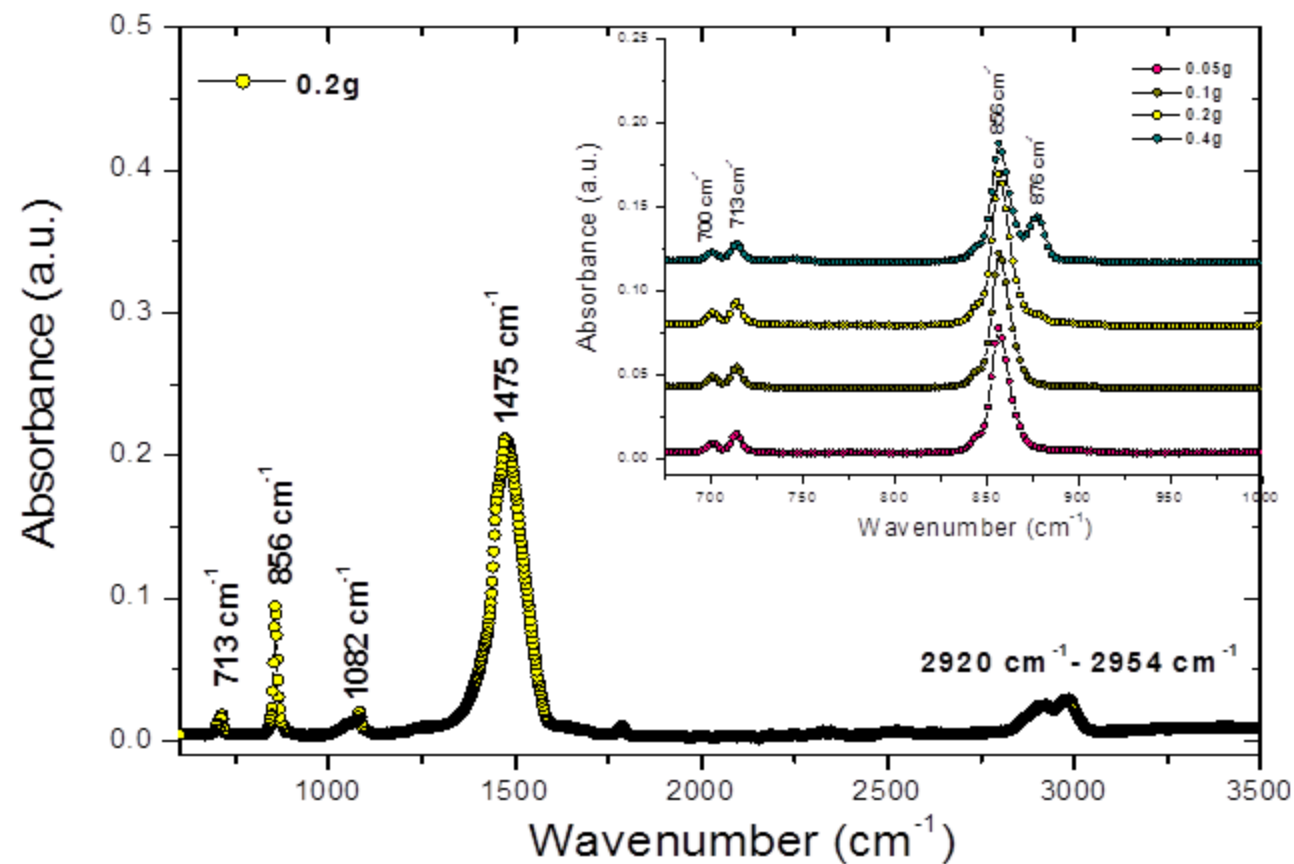
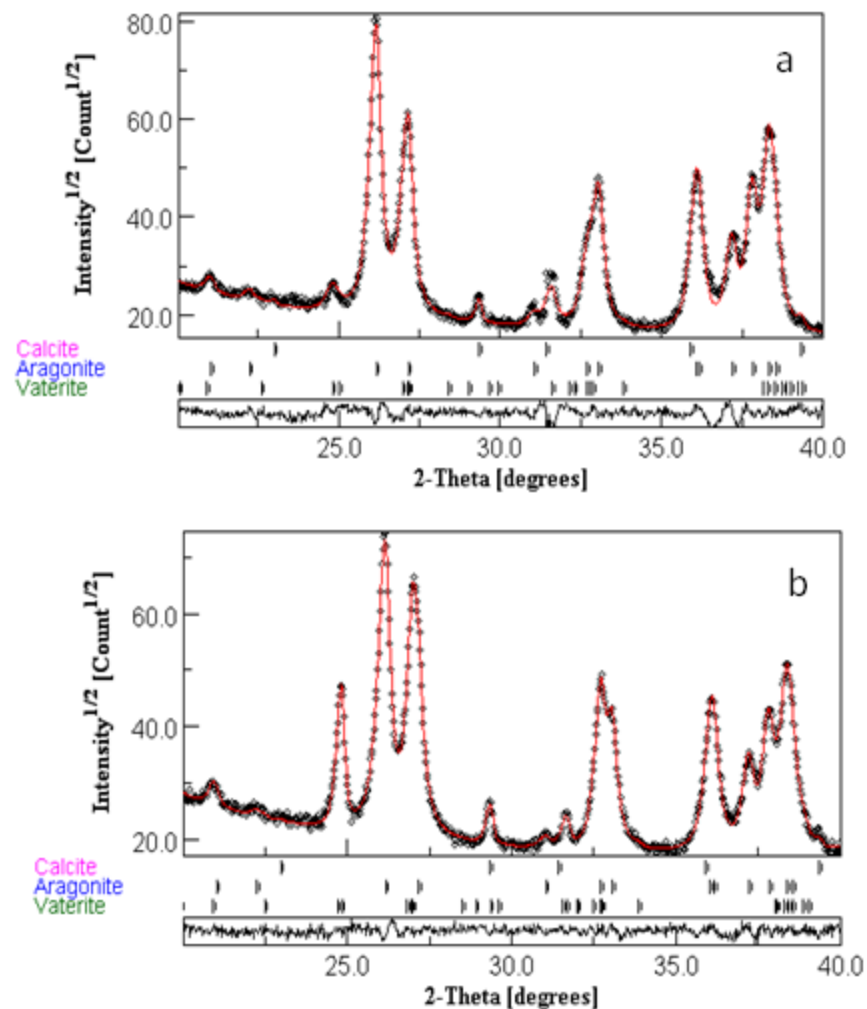


Fig.8:

Left: FT-IR spectrum of CaCO_3 particles nucleated with soap :
0.05g, 0.1 g, 0.2 g, 0.4 g at 80°C .

Right: Observed, calculated and difference curves after Rietveld refinement :
(a) 80°C with 0.2 g soap ; (b) 80°C with 0.4 g soap.



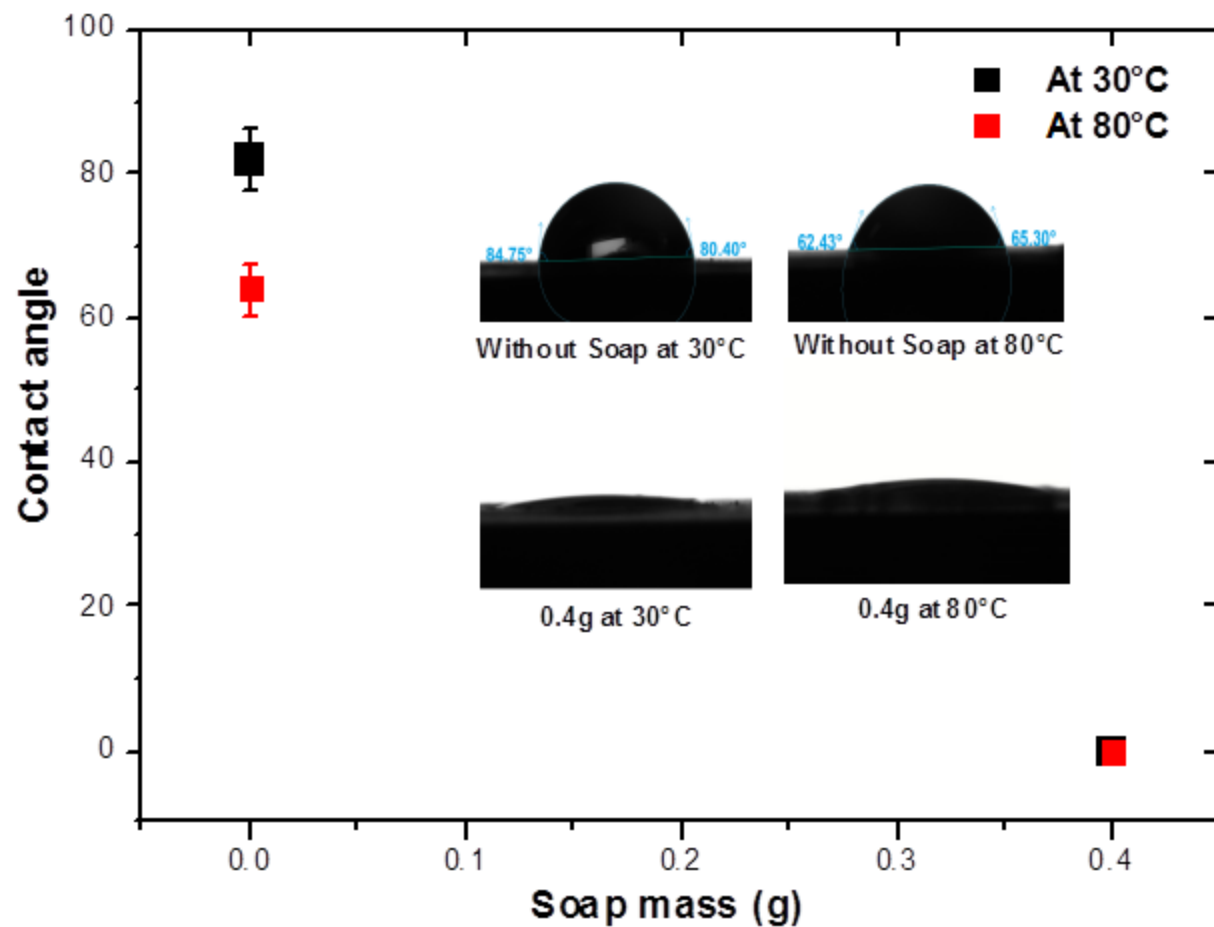
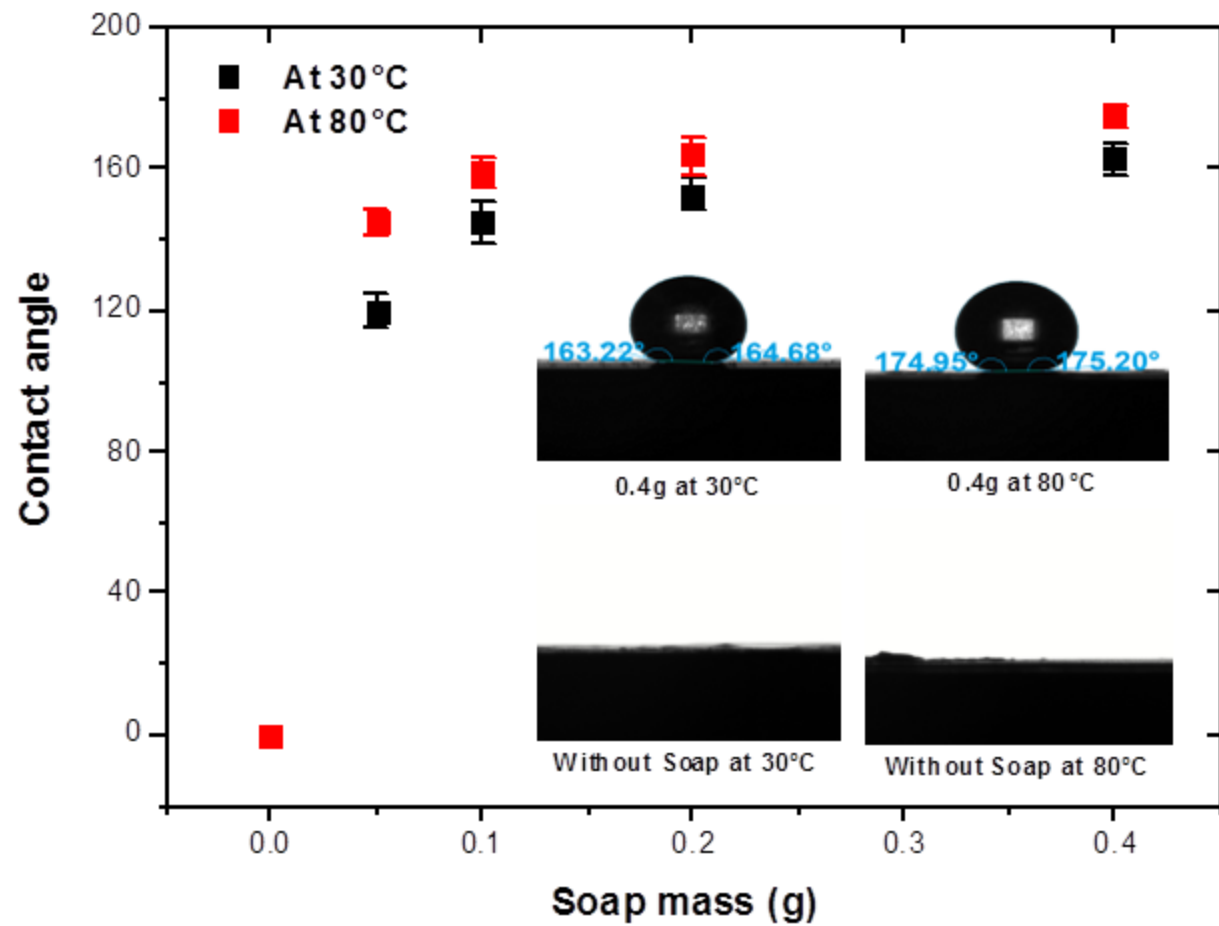


Figure.9: Evolution of the water (left) and oil (right) contact angle as a function of the added soap mass.

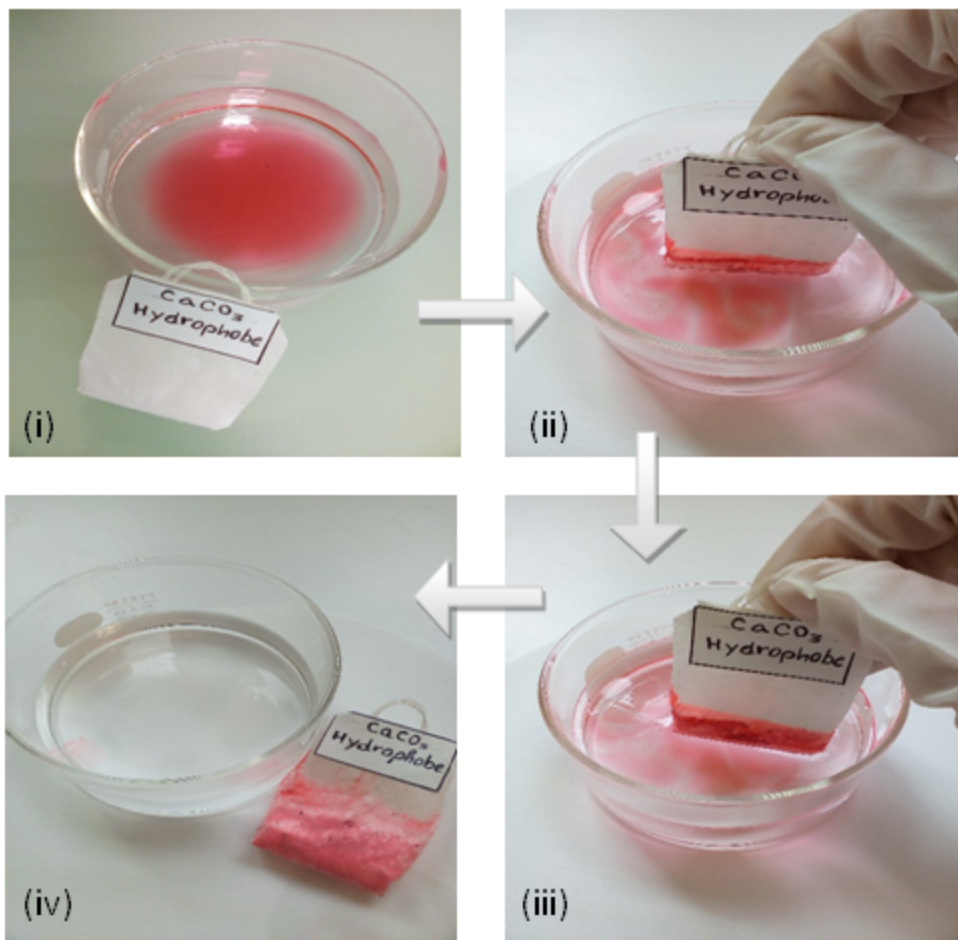


Figure.10: Selective removal of oil in a spill on water by hydrophobic CaCO₃:
(i) oil at the surface of water (ii and iii) oil gradually absorbed by the pouch containing hydrophobic CaCO₃ (iv) clean water and oil completely absorbed by the pouch.

	Absorption band	Vibration mode
Calcite [19, 10, 47-50]	712 848 877 1435	Doubly degenerate In-plane OCO deformation bending CO ₃ out-of-plane bending CO ₃ Out-of-plane bending Doubly degenerated asymmetric C-O stretching
Vaterite [19, 13, 47-51]	744 849 877 1090 1424 1450 1465 1490	Doubly degenerate In-plane OCO deformation bending CO ₃ out-of-plane bending CO ₃ Out-of-plane bending Symmetric C-O stretching C-O stretching Doubly degenerated asymmetric C-O stretching Doubly degenerated asymmetric C-O stretching Doubly degenerated asymmetric C-O stretching
Aragonite [4, 19, 48-50, 52]	700 712 854 1082 1475 1486	Doubly degenerate In-plane OCO deformation bending Doubly degenerate In-plane OCO deformation bending CO ₃ out-of- plane bending Symmetric C-O stretching Asymmetric C-O stretching C-O stretching
Olive Oil [53-55]	723 1097 1118 1163 1239 1377 1465 1743 2853 2922 3007	-(CH ₂) _n - rocking -C-O stretching -C-O stretching -C-O stretching -C-O stretching -C-H (CH ₃) symmetric bending -C-H (CH ₂) bending -C=O stretching -C-H symmetric stretching -C-H asymmetric stretching =C-H stretching
Soap [56]	721 1045 1420 1440 1460 1557 1650 2852 2920 2954 3383	-(CH ₂) _n -rocking -C-O stretching =C-H bending (rocking) -C-H (CH ₃) asymmetric bending -CH ₂ -bending Carboxyl (-COO ⁻) -OH bending -CH ₂ symmetric stretching -CH ₂ asymmetric stretching -CH ₃ symmetric stretching -OH stretching

Table I: Specific frequencies in cm⁻¹ reported for the different materials used in this study

